A molecular level simulation of a twisted nematic cell

Matteo Ricci[1], Marco Mazzeo[1]*,
Roberto Berardi[1], Paolo Pasini[2] and Claudio Zannoni[1]†

[1]Dipartimento di Chimica Fisica e Inorganica, and INSTM–CRIMSON,

Università di Bologna, viale Risorgimento 4, 40136 Bologna, ITALY

[2]Istituto Nazionale di Fisica Nucleare (INFN), Sezione di Bologna,

via Irnerio 46, 40126 Bologna, ITALY

Abstract

We have performed a Monte Carlo simulation of a sub–micrometric twisted nematic cell with nearly 10^6 particles using an off–lattice molecular model of a liquid crystal. This computer experiment is a proof of principle that molecular models can be pushed to the limit of the system sizes addressable with finite elements models thus bridging the mesoscopic gap for multiscale modelling while providing a direct molecular level view of the working of the display. This approach, that allows a direct prediction of molecular organisations, properties, and responses of device systems without the requirement of prior estimate or knowledge of material properties (*e.g.* elastic constants), is particularly important in view of simulating materials and devices for which these quantities are not known. Results for the molecular organisation are discussed, with particular regard to its helical nature in the field–*off* state.

1   Introduction

One of the most successful stories in advanced materials must be that of liquid crystals (LC) displays [1]. The basic concept behind the most classical device, the twisted nematic (TN) display [2], is that a pixel is activated by a change of molecular organisation in the few micrometre thick cell from a surface dominated (*off* state) to a field–driven one (*on* state). Thus, an initial configuration of the local preferred direction (the director) is established between two perpendicular aligning surfaces (*e.g.* rubbed glass or polyimide) that confine the LC. An experimental fact is that linearly polarised light is going through the pixel in this

---

*current address: Centre for Computational Science, University College of London, 20 Gordon St., London WC1H OAJ, UK; email: Marco Mazzeo ⟨m.mazzeo@ucl.ac.uk⟩

†corresponding author; email: Claudio Zannoni ⟨claudio.zannoni@unibo.it⟩

off state and this is compatible with a microscopic helical configuration of the local director orientation which rotates the plane of polarisation. If the chosen LC has a positive dielectric anisotropy and a suitable voltage is applied across the cell in correspondence of a pixel, then polarised light does not go through, compatibly with a monodomain organisation. When the field is switched off the original organisation is re–established thanks to elastic restoring forces and surface interactions.

To the best of our knowledge there is little evidence that the molecular level organisation in absence of a field is actually a uniform helix. For instance, the classic textbook picture is that of uniformly twisted layers that do not actually exist as such as the organisation remains that of a nematic without positional order or layering.

Moreover, the way the twisted organisation is established is not obvious, for instance after an *off–on–off* cycle does the reorganisation re–start from the centre of the cell or from the surface? Is a uniform helix really formed? Or how helical is the structure?

Computer simulations of similar TN device setup have been performed by using lattice models [3, 4, 5, 6, 7], with fixed spins positions. However, simulation studies based on models where particles have both positional and orientational degrees of freedom (off–lattice) have not been reported so far.

In this work we tackle some of these questions by setting up a molecular resolution off–lattice model of a TN cell containing $\mathcal{O}(10^6)$ particles and simulating its behaviour using a Monte Carlo (MC) method. This corresponds to samples two orders of magnitude larger than the typical ones currently studied with off–lattice molecular models, and thus presents some significant computational challenges with present day computers.

In this paper, after introducing our model $\pi/2$ TN cell, we shall discuss the technical details of the specific parallel MC code we have developed for this purpose. In the second part of the manuscript we shall show our simulation results both for the spontaneous formation of a supermolecular helical structure in the *off* state, and the commutation of the central pixel to the *on* state by an electric field applied across the TN cell.

2 Model

Standard modelling of LC electro–optical devices uses continuum descriptions [8, 9] relying on input parameters for elastic constants, viscosities, and other material constants. These data are not available for novel materials (*e.g.* biaxial nematics [10]). Atomistic simulations [11], where molecules are described at full atomic resolution, would be the natural alternative approach to use, but the sample sizes required to realistically model the distance and time scales of a TN cell are currently well beyond available and foreseeable computational resources. At the other extreme we find lattice models [3, 4, 5], where every site represents a uniformly aligned monodomain formed by hundreds of molecules. In this case the simplicity of the model allows the simulation of mesoscopic size systems, even though at the price of disregarding possibly relevant positional degrees of freedom. Instead, we are not aware of any computer simulation study based on off–lattice models where molecules are explicitely described with simple geometrical shapes and suitable interaction energies. Here we have modelled the LC molecules inside the cell using the Gay–Berne (GB) potential [12, 13, 11] which is *de facto* a standard and well established model for liquid crystalline systems, giving the correct temperature dependence of order parameters, and the sequence of phase transitions for many model mesogens [14]. The GB pair potential is an anisotropic Lennard–Jones which can be written

as

$$U_{GB}(\mathbf{r}, \hat{\mathbf{u}}_1, \hat{\mathbf{u}}_2) = 4\epsilon_0\, \epsilon(\mathbf{r}, \hat{\mathbf{u}}_1, \hat{\mathbf{u}}_2)\left[u^{12}(\mathbf{r}, \hat{\mathbf{u}}_1, \hat{\mathbf{u}}_2) - u^6(\mathbf{r}, \hat{\mathbf{u}}_1, \hat{\mathbf{u}}_2)\right], \qquad (1)$$

where the terms $u(\mathbf{r}, \hat{\mathbf{u}}_1, \hat{\mathbf{u}}_2) \equiv \sigma_c/(r - \sigma(\mathbf{r}, \hat{\mathbf{u}}_1, \hat{\mathbf{u}}_2) + \sigma_c)$, contain the anisotropic contact function $\sigma(\mathbf{r}, \hat{\mathbf{u}}_1, \hat{\mathbf{u}}_2)$ which estimates of the contact distance between two ellipsoids [15, 16]. The contact function depends both on the axes σ_x, σ_y, and σ_z of the ellipsoid, and on the orientations $\hat{\mathbf{u}}_1$, $\hat{\mathbf{u}}_2$ for the long molecular axes (as unit vectors), and the intermolecular vector $\mathbf{r} = \mathbf{r}_2 - \mathbf{r}_1$, with $\mathbf{r}_i = (x_i, y_i, z_i)$.
The interaction function $\epsilon(\mathbf{r}, \hat{\mathbf{u}}_1, \hat{\mathbf{u}}_2)$ defines the attractive well depth, and depends on the axes σ_i, on the three interaction coefficients ϵ_x, ϵ_y, and ϵ_z defining the relative energy for the *side–by–side*, *face–to–face*, and *end–to–end* configurations of a pair of particles [17, 18], and on the orientations. The empirical parameters σ_c, μ, and ν modify the width and depth of the attractive wells. The constants σ_0, and ϵ_0 define the length and energy scales. We represent the nematic molecules as uniaxial GB elongated ellipsoids, and use a parameterisation already employed in past works [19], namely $\sigma_x = \sigma_y = \sigma_c = 1\ \sigma_0$, $\sigma_z = 3\ \sigma_0$, and $\epsilon_x = \epsilon_y = 1\ \epsilon_0$, $\epsilon_z = 0.2\ \epsilon_0$, and $\mu = 1$, $\nu = 3$, giving isotropic (I), a wide nematic (N) phase, and smectic (Sm) at low temperatures. Here we are interested in the nematic mesophase, so we have worked at constant dimensionless temperature $T^* = k_B T/\epsilon_0 = 2.8$, and density $\rho^* = \sigma_0^3 N/V = 0.3$, with $\sigma_0 \approx 6 \times 10^{-10}$ m, and $\epsilon_0 \approx k_B 100$ K, which correspond to a room temperature nematic organisation with average bulk order parameter $\langle P_2 \rangle = 0.806 \pm 0.012$ [19].
A geometrical scheme of the sample setup for the TN cell simulation is given in Figure 1. The internal dimensions of the TN cell were set to $L_x = L_y = 167.7906\ \sigma_0$, and $L_z = 93.8604\ \sigma_0$, which roughly correspond to a $0.100 \times 0.100 \times 0.067\ (\mu m)^3$ volume, available to the $N_{lc} = 787320$ GB particles modelling the nematic fluid.
To model a $\pi/2$ TN cell with planar aligning surfaces we have used periodic boundaries along the laboratory X, and Y directions, and confining surfaces along Z consisting in two slabs cut from a lattice of parallel GB particles with thickness $w_z = 9\ \sigma_0$ corresponding to nine crystalline layers. The positions and orientations of the confining GB particles were kept fixed during the MC simulation. The two surfaces were prepared with orthogonal directions of molecular alignment, and an additional small pretilt angle of $\theta = 5°$, was imposed on both surfaces to remove energetical degeneracy [20]. The surface particles had the same parameterisation of those modelling the nematic fluid, *i.e.* we assumed the surface–fluid interactions to be of the same entity of the fluid–fluid ones. The overall MC sample size was $N = 944784$ GB particles (with $N_{lc} = 787320$ for the nematic, and $N_w = 157464$ for the surfaces).

3 Computational methodology

The MC or molecular dynamics simulation of a realistic TN display is a very challenging task because the several micrometres size, and the milliseconds response times of the device are well beyond the conventional spatial and temporal ranges accessible with standard computer simulations. We have chosen to employ the MC method under canonical conditions which, even for molecules much more complex than the simple particles used here, is expected to have some advantages in exploring phase space [21, 22]. However, performance problems arise when using MC methods with very large systems because the standard Metropolis algorithm

for updating molecular configurations proceeds by generating random sequences of single–particle moves in an intrinsically sequential way. General multi–particle moves are possible but unless performed with a biasing scheme [23] they may suffer from poor sampling statistics. Recently, effective parallel MC techniques with modified Markov chains for large off–lattice samples have been introduced [24, 25] relying on uncorrelated particles which can be moved simultaneously by different processors working in parallel. Here we have developed a special purpose parallel code based on an algorithm similar to that described in Refs. [24, 25]. The basis of the method is that if the sample is sufficiently large and the pair interaction potential is short–ranged (*i.e.* with a dependence on distance r^{-n} with $n > 3$) it is possible to introduce a potential cutoff distance r_c. This cutoff is possible also if the effective long–range interactions are shielded [26], and $g(r)$ levels off to the asymptotic limit of 1 for small distances r, and the system is far from first order phase transitions. In this case two (or more) not directly interacting particles (*i.e.* at distance $r > r_c$) can be moved independently without affecting the physics of the system. This is thus a special case of multi–particle move which does not bias the standard Metropolis sampling scheme and we have taken advantage of this.

The case of GB interactions is fairly favourable since they fall off as r^{-6}, and this allows to partition the sample into non interacting sub–domains. In detail, for a MC simulation concurrently using P processors, the whole cell (including the surfaces) is subdivided into $P = N_x \times N_y \times N_z$ virtual domains with sides d_x, d_y, and d_z equal or larger than $r_c + r_{max}$, where r_{max} is the width of the uniform distribution used to sample random translational MC moves. Every processor independently evolves particles only in a given domain (and also uses its own sequence of random numbers). Each domain is further subdivided into eight local sub–domains (three–dimensional octants), labelled according to their position. At each MC sweep a sub–domain label is collectively selected, and each processor attempts the MC move of a randomly selected particle in its local sub–domain. Due to this spatial decomposition the $r > r_c + r_{max}$ constraint is always fulfilled by all $P(P-1)/2$ pairs, even for the largest random displacements, and clashes are prevented by design. After a MC move the inter–processor exchange of updated coordinates is made only to the seven CPUs managing the domains adjacent to the sub–domains where the particle moves have been accepted [24, 25]. This concurrent P–particle Markov chain becomes computationally advantageous if an efficient underlying mapping algorithm does the necessary bookkeeping of the various domains and sub–domains populations, allowing a fast computation of pair interactions. In practice, a standard linked–cells algorithm with particle binning based on a $41 \times 41 \times 27$ partition of the whole TN cell, and optimised handling of periodic boundary conditions, has been used, corresponding to linked–cells with sides $c_x = c_y = 4.092\ \sigma_0$, and $c_z = 4.143\ \sigma_0$ (see Figure 1). This algorithm has demonstrated sufficient scalability and we have run all our MC simulations using a pool of $P = 128$ processors with $N_x = N_y = 4$ and $N_z = 8$, and using the MPI message passing libraries. It might be worth noting that, even though we have focussed and successfully employed MC, in perspective MD could also be used, as several efficient parallel MD engines for off–lattice molecular models are becoming publicly available. For instance, the biaxial [17, 18] and RE–squared [15] variants of the GB potential are now included in the LAMMPS [27, 28] open–source code.

To compute the optical image of transmitted polarised light across the simulated cell (including crossed polarisers), we have used the Stokes–Mueller 4×4 matrix formalism as described in [3, 4, 5, 29, 30]. Even though the rigorous solution of the Maxwell equations [31] would be necessary to reproduce finer effects, the simple geometrical optics based on Stokes–Mueller

matrices [29, 30] has proved to be quite adequate and sufficient to provide an overall description of the optical transmission of anisotropic planar media like a TN cell. In our model calculation we have considered the refractive indexes for the 5–cyano–biphenyl (5CB), namely the ordinary $n_o = 1.5$, and extraordinary $n_e = 1.7$, and a transmitted wave length of $\lambda = 500$ nm.

4   Simulation results

The analysis of the MC simulation results is divided in two stages. First we show the results of the relaxation experiment leading to the spontaneous formation of a twisted organisation. Then we move to the response to an external switching field and the computation of optical transmission properties.

4.1   Spontaneous helix formation

We have investigated the spontaneous formation of a helical organisation inside our TN cell. The canonical, NVT MC simulation has been started from a configuration of rod–like GB particles uniformly aligned along the laboratory Z axis (*i.e.* perpendicular to the confining surfaces, see Figure 2–b). This unfavourable starting configuration resembles the one obtained ideally after switching off a field that has aligned the nematic (dark pixel). The sample was allowed to relax by performing 1.76×10^6 sweeps, each consisting of N attempted rotational and translational MC moves. The response under an external switching field described into the next section was simulated running additional 1.12×10^6 sweeps starting from the final configuration of the relaxation process (see Figure 2–c). The sampling ranges for translational $[-t_{max}/2, t_{max}/2]$ and orientational $[-\theta_{max}/2, \theta_{max}/2]$ moves were automatically adjusted during the MC run to give an average acceptance ratio of 0.4 for the roto–translational moves, resulting in typical $t_{max} = 0.08 \ \sigma_0$, and $\theta_{max} = 13°$ values. Orientational moves were randomly sampled using the standard Barker–Watts [32] algorithm.

The relaxation process was followed by monitoring the evolution of the average potential energy per particle $\langle U_{GB} \rangle$ of the nematic sample, and the second rank order parameter $\langle P_2 \rangle = \langle (3(\hat{\mathbf{u}}_i \cdot \hat{\mathbf{n}})^2 - 1)/2 \rangle$, computed with respect to the overall sample director $\hat{\mathbf{n}}$ (given as a unit vector) using the standard algorithm of diagonalisation of the order matrix [33]. The simulation was continued until no systematic drift was observed in these observables (see Figures 3–a and 3–b). In Figure 3–a we see that the potential energy grows in few MC ksweeps from $-11.24 \ \epsilon_0$ to $\approx -7.6 \ \epsilon_0$, then relaxes to a practically constant value. Also for the $\langle P_2 \rangle$ plot of Figure 3–b the starting uniform director distribution is destroyed in a few MC ksweeps, and the overall $\langle P_2 \rangle$ drops down from 1 to ≈ 0.5.

More insight on the molecular organisation across the cell and its evolution was obtained dividing the TN cell into N_s virtual parallel slabs of thickness $\Delta z = L_z/N_s$ (here $N_s = 30$) to compute specific local order parameters $\langle P_2 \rangle_s$ and orientational correlation functions between pairs of particles belonging to different slabs (*i.e.* with different z_i elevation). In our cell each of the $N_s = 30$ slabs has thickness $\Delta z = 3.729 \ \sigma_0$, *i.e.* approximatively 25% thicker than the length of the mesogenic particles, and contains on average ≈ 26100 GB particles. After the relaxation of the uniformly aligned initial configuration the order parameters $\langle P_2 \rangle_s$ relative to the local director $\hat{\mathbf{n}}_i$ of each planar slab remain essentially constant across the sample and over the simulation run (not shown here). In this part of the MC evolution the GB particles which are not in proximity of the surfaces equilibrate to a plateau $\langle P_2 \rangle_s \approx 0.79$,

which is within the error bar of the $\langle P_2 \rangle = 0.806 \pm 0.012$ average value found for the bulk systems [19] at the same temperature and density. Thus, the presence of the aligning surfaces and the formation of the twisted helical structure does not affect, for samples of this size, the magnitude of the orientational ordering in the centre of the cell [34], but only the direction of the local director. This result is consistent with a physical picture of gradual re–alignment of small ordered regions/clusters whose local properties are not largely perturbed by the overall helical organisation [35].

The same is also true for the density distributions of centres of mass of the nematic particles $g(z)$ (not shown here) which show that during the entire relaxation stage the sample was nematic and devoid of positional ordering, apart from approximatively 4 to 5 surface–induced smectic layers in the proximity of the planar surfaces. This is fairly commonly observed in simulations of nematics close to aligning surfaces [36, 37].

The formation of a helical structure can be monitored by computing order parameters giving the orientation of the local directors with respect to that of a perfectly helical organisation (with a pitch equal to four times the $\pi/2$ cell thickness L_z). The centre of every i-th slab has assigned to it a specific reference orientation $\hat{\mathbf{t}}_i$ corresponding to the ideal helix, and for every configuration a local director $\hat{\mathbf{n}}_i$ can be obtained from the standard algorithm of diagonalisation of an order matrix for the molecular $\hat{\mathbf{u}}_i$ axes. The local helical order parameters $\langle P_2 \rangle_h$ [3] are defined as

$$\langle P_2 \rangle_h = \frac{1}{N_s} \sum_{i=1}^{N_s} P_2(\hat{\mathbf{n}}_i \cdot \hat{\mathbf{t}}_i), \tag{2}$$

and a fully formed helix corresponds to $\langle P_2 \rangle_h \approx 1$. In Figure 4 we show how the disruption of the initial uniform director distribution takes place during the relaxation from uniformly aligned to twisted nematic. The starting phase of the process appears to be the alignment of the nematic slabs closest to the surfaces, leaving the central portion of the $\langle P_2 \rangle_h$ profiles essentially unaffected. This transformation takes place in few thousands MC sweeps, and gradually propagates from both directions towards the centre of the cell. The ensuing reorganisation process of the central region is much longer (still at constant $\langle P_2 \rangle_s$), and the number of MC sweeps required to reach $\langle P_2 \rangle_h \geq 0.75$ is now of the order of 10^6 sweeps (approximatively two orders of magnitude longer). These order parameter values are significantly smaller than 1 hinting that the simulated cell does not attain a perfectly uniform helical organisation across the sample, and the local directors $\hat{\mathbf{n}}_i$ have some sort of deviation from the geometrical pattern described by the $\hat{\mathbf{t}}_i$ orientations. This can be quantified by computing the chiral correlations [37] between nematic particles at a certain elevation z with those near the aligning surfaces

$$S^{221}(z) = -\frac{\sqrt{3}}{\sqrt{10}(L_x L_y \rho)^2} \langle \delta(z - z_j + Z_1)(\hat{\mathbf{u}}_i \cdot \hat{\mathbf{u}}_j \times \hat{\mathbf{z}}_{ij})(\hat{\mathbf{u}}_i \cdot \hat{\mathbf{u}}_j) \rangle_{i,j}, \tag{3}$$

where the subscript i refers to the particles in the first slab (centred at laboratory Z_1), while j spans the remaining GB particles in the sample. The unit vector $\hat{\mathbf{z}}_{ij}$ is parallel to the laboratory Z axis when $z_j > z_i$ (as in our case), otherwise it is antiparallel. We see in Figure 5 how the chiral correlation gradually and steadily develops during the relaxation starting from the surfaces towards the cell centre, and as the simulation progresses, it slowly approaches (some sort of) asymptotic limiting profile which is however still far from the ideal helical one.

We also see that the small initial structural asymmetry around $Z = 32\ \sigma_0$ due to a local fluctuation is eventually lost, as expected, at the end of the relaxation process.

Yet another way of characterising the director distribution in the various planar slabs is that of monitoring the azimuthal angles ϕ_i formed by the projection of the local directors $\hat{\mathbf{n}}_i$ on the XY and YZ laboratory planes. The azimuthal angles ϕ_{xy}, and ϕ_{yz} change during the relaxation process, and Figure 6–a shows how the initial $\phi_{xy} = 0°$ constant value evolves and eventually approaches fairly closely the ideal linear profile for a geometrically perfect helical organisation. The deviations from the ideal helical structure are due to the tilt out of plane of the local directors $\hat{\mathbf{n}}_i$, shown in Figure 6–b, where we see that even after 1.76×10^6 sweeps the central slabs have a residual director tilt $\phi_{yz} \approx 25°$. As will be shown later this reflects into the response to an external field mainly arising from the central slabs. For both azimuthal angles profiles the changes taking place during the MC evolution start in the slabs at the surface boundaries and then propagate towards the central ones.

A direct, molecular level, representation of these arguments is given by the sample snapshots of Figure 7 which clearly show how the structural transformation takes place under effect of the two opposite driving forces given by the tendency to align parallel to the closest surface, and that of minimising the elastical strain imposed by the $\pi/2$ cell twist. We see from the colour coding of the orientations that the director distribution is not perfectly uniform and small local fluctuations are present. To make the relation to the actual optical performance more clear, we also show images (Figure 7) of the linearly polarised light transmitted across the TN cell, including the crossed polarisers, computed as described in Refs. [3, 4, 5]. These show how a transparent state is obtained only in the final part of the MC relaxation, and that the local transmittance can fluctuate several times from opaque to transparent and back before the final bright state is achieved. These snapshots also show that whatever the structure within the cell, the particles close to the confining surfaces remain parallel to the alignment direction. These arguments are made more quantitative in Figure 8 where we plot the total cell transmittance both for the field–*off* MC relaxation from uniformly aligned, and the virtual switching experiment described in the next section. In particular, the leftmost portion of Figure 8 shows a two–regimes relaxation, characterised by an initial low–transmittance state (lower than 5%), which is maintained for approximatively 5×10^5 sweeps, and followed by a second stage with quite larger positive slope of the transmittance curve lasting for roughly 1×10^6 sweeps until it begins levelling off in correspondence of an $\mathcal{T} \approx 90\%$ transmittance of the entire cell.

4.2   Central pixel switching

To perform the field–induced virtual switching experiment [35] we have gridded the XY plane of the confining surfaces into a 3×3 square pattern of pixels, and mapped the x_i, and y_i coordinates of the nematic particles accordingly. The MC switching experiment is characterised by the application, in the cell region corresponding to the central pixel, of a (electric) field parallel to the laboratory Z axis, and has been performed by running 1.12×10^6 sweeps starting from the last configuration of the previous relaxation process. The beginning of the virtual experiment is indicated in Figures 3 and 8 by a vertical black line at 1.76×10^6 sweeps. In practice, particles in the central pixel were subjected to an extra potential energy term U_F modelling the dielectric (second rank) coupling of the molecular $\hat{\mathbf{u}}_i$ axis with the external field, according to the equation

$$U_F = -\xi_F \left[\frac{3}{2}(\hat{\mathbf{u}}_i \cdot \hat{\mathbf{Z}})^2 - \frac{1}{2} \right], \tag{4}$$

where the field–coupling constant is defined as $\xi_F = \varepsilon_0 \Delta\epsilon V_0 E^2/3$, with $\Delta\epsilon$ the susceptibility anisotropy, V_0 the molecular volume, $\hat{\mathbf{Z}}$ the direction of the electric field, and ε_0 the vacuum permittivity. The coupling coefficient we used was $\xi_F = 0.05\ \epsilon_0$, roughly corresponding (with $\Delta\epsilon = 12$) to an applied field intensity of $E \simeq 7.6 \times 10^7$ Vm^{-1}, approximately one order of magnitude bigger than those used in real TN devices, and nonetheless giving a U_F energy much lower (typically $< 4.5\%$) than the U_{GB} term. In Figure 3–a we see that the GB energy does not drift during the switching experiment, and this is consistent with a cartoon of a weak coupling between external field and nematic molecules. We also see that the overall order parameter of Figure 3–b exhibits a rather small decrease after the central pixel re–alignment has taken place.

Again, we have used local averages and correlations to characterise the switching process. In Figure 9 we report the profiles for the helical $\langle P_2 \rangle_h$, and the field direction $\langle P_2 \rangle_e$ order parameters. We see that the central slabs of the switched pixel do not completely align along the laboratory Z direction (*i.e.* they do not attain the limiting $-1/2$ value for $\langle P_2 \rangle_h$, and 1 for $\langle P_2 \rangle_e$) and a certain amount of orientational disorder remains. In particular, the central slab has the largest degree vertical alignment ($\langle P_2 \rangle_e \approx 0.6$) but still lower than the extent ($\langle P_2 \rangle \approx 0.8$) found in a bulk nematic system at the same temperature and density [19]. On the other hand, the slabs closer to the confining surfaces maintain during the entire switching process a positive $\langle P_2 \rangle_h$ (Figure 9–a), and a negative $\langle P_2 \rangle_e$ (Figure 9–b). The 8 external pixels are not globally influenced by the field, and the profiles of the local order parameters do not change during the virtual switching experiment (not shown here), *i.e.* boundary effects are negligible for this 3×3 switching pattern.

Figure 10–a shows an interesting residual helical structuring in ϕ_{xy} (*i.e.* in the n_x, and n_y components of the local directors) which corresponds to the initial helical distribution prior to the switching on of the external field. However, the noisy profiles of Figure 10–a suggest that the plotted ϕ_{xy} values are an artificial amplification of small and fluctuating events, and at the time being we are not able to discriminate between a true *"memory"* effect and boundary effects originating from the *on* pixel being completely surrounded by *off* ones (other switching patterns may produce different behaviour). This phenomenon may be important in the restoring of the helical configuration after the aligning field is switched off, since this process should be governed by the twist elastic constant, and only indirectly by the aligning affect due to the confining surfaces. The ϕ_{xy} profiles for the external pixels are unaffected by the switching experiment (not shown here).

The chiral pair correlations in the central pixel are destroyed in approximatively 5×10^5 sweeps after switching on the field (see Figure 10–b). In the second half of the virtual experiment the $S^{221}(z)$ levels to a broad M–like profile, and the residual chiral correlations are mainly concentrated into the external slabs where the slope of $S^{221}(z)$ is larger. The chiral pair–correlation profiles for the 8 external pixels are unaffected by the switching experiment (not shown here).

The organisation at the end of the virtual experiment is graphically rendered by the snapshot of Figure 11–a, where the TN cell has been vertically sliced at $Y = 0$ to expose the orientational structure of the central pixel. The colour coding of the particles shows that the internal core is fairly aligned with the laboratory Z axis, while the intermediate nematic and boundary slabs have not responded to the same extent to the external perturbation. In our simulation there

is no gap between pixels [20] and we see that the aligned molecules of the field–*on* pixel tend to align those of the neighbouring ones, and the snapshot of the cross–section in Figure 11–a also shows that the central oriented region has a somewhat globular shape, which slightly spreads to the neighbouring pixels where the external field is absent. This can also be seen from Figure 11–b giving the transmittance along Z of linearly polarised light across the whole TN cell. We see that the dark opaque area extends irregularly over the boundaries of the central pixel, which also has a not uniform degree of light extinction, with an average value of 91%.

The commutation from transparent to dark is shown in Figure 12 where we see how the transmittance of the central pixel decreases during the virtual MC experiment. The dark area develops in the core of the pixel, where the effects due to the external pixels are smaller, and gradually intensifies and enlarges towards the boundaries to cover the entire field–*on* cross–section and beyond. The total cell transmittances for both central and external pixels are given by the right portion of Figure 8. While light passing through the external pixels decreases less than 10% from the starting value, for the central pixel it smoothly diminishes from 90% to 10% in 1×10^6 sweeps.

5 Discussion and conclusions

This paper has two main objectives. The first is to show that fairly massive parallel computing can now be applied to push the application of coarse–grained molecular resolution simulations to the modelling of fairly realistic devices. We have successfully employed to this end a specially written MC code to perform an extensive simulation of a TN cell containing $\mathcal{O}(10^6)$ GB mesogenic particles.

The second objective is to gain insight on the actual microscopic working of an important electro–optical device that is commonly assumed to correspond to a uniformly helical structure letting plane polarised light through a pixel, and turning, under the effect of a suitable field, to a vertical monodomain that has the effect of shutting the transmission through crossed polariser.

We have found that this picture is somewhat incomplete and perhaps even misleading. We have seen from MC simulations that a uniform helix is not formed at once when an initial vertical monodomain is relaxed under the effect of the two aligning surfaces and the nematic intermolecular interactions. Rather, two uniformly aligned domains start to grow under the orienting effect of the two perpendicular surfaces and only when the two domains meet is the twisted structure formed with the consequent passage of light.

Since we perform Monte Carlo simulations the natural evolution variable is not real time but MC sweeps. Nonetheless, we believe these MC simulations have some predictive power not only for the initial and final equilibrium states of a virtual experiment, but also for the evolution between the two states. Since our MC moves correspond to single–particle physical movements such as translations and rotations, we can essentially map the MC evolution onto a stochastic jump process for the molecules. Thus we may expect that the ratio between the number of MC sweeps required for the *on–off* and *off–on* processes can be approximatively compared to the experimental one for a device of similar geometry, and measured in real time units. In particular, we also expect that the initial low–transmittance stage we have observed (lasting approximatively for 1/3 of the entire relaxation run), may be experimentally investigated. Indeed similar experiments have been performed by Toriumi and coworkers [38, 39, 40] using

a variant of time–resolved spectroscopic ellipsometry (TRSE) where the polarisation of light modulated by the interfacial layer of a nematic (5CB) in an antiparallel homogeneously aligned cell has been measured. In that case two regimes were also found for the relaxation of the director distribution of the nematic, previously homeotropically aligned with a field, to the homogeneous state determined by the boundaries. The two regimes, successfully modelled in [40] with a Frank–type continuum theory consist, similarly to what we have found here (albeit for a different cell geometry), to a fast relaxation of the nematic close to the surface and a much slower one for the one in the cell centre. The fact that such an agreement is found starting from both molecular and continuum descritions is a practical confirmation that we have essentially closed the gap between the two treatments.

As for the twisted structure obtained, we have examined its character in detail, finding that it approximates but never fully assumes a truly helical organisation and we have quantified this with a helical order parameter and a chiral correlation function. We have also studied the field–*on* realignment process and found that it starts from the middle of the TN cell taking a smaller number of MC sweeps ($\approx 1.1 \times 10^6$ sweeps) to complete than the previous field–*off* relaxation. We find that even applying the field to a square area of the display, the black pixel resulting is somewhat more fuzzy as a consequence, at least for our cell configuration, of the aligning effect that the region of field–aligned molecules exerts on the neighbouring molecules not subject to the field and *vice versa*. The process does not lead, however, to significant changes of the overall order and structure, or average transmittance, of the domain surrounding the field–*on* one.

As a final statement, even if the effort and resource needed to perform this type of simulations is at the moment huge, we would like to point out some features that could make the technique quite important in the near future. The first is the possibility of studying non–uniform, rough, or nanostructured confining surfaces, or surfaces containing a given concentration of defects and seeing their effect on the device. The second is the possibility of studying more exotic displays, *e.g.* those currently planned with biaxial nematics [41, 10] where the chemical structure, or the molecular organisation and its changes under the effect of an applied field are less known and obvious, while at the same time the material constants are very numerous and unknown. The molecular technique presented here should allow in these cases to predict the workings and the performance of a device starting only from the knowledge of molecular parameters, avoiding the use of continuum level theories.

6   Acknowledgements

References

[1] P. Semenza, *Nature Photonics*, 2007, **1**, 267–268.

[2] M. Schadt and W. Helfrich, *Appl. Phys. Lett.*, 1971, **18**, 127–128.

[3] E. Berggren, C. Zannoni, C. Chiccoli, P. Pasini, and F. Semeria, *Int. J. Mod. Phys. C*, 1995, **6**, 135–141.

[4] C. Chiccoli, P. Pasini, S. Guzzetti, and C. Zannoni, *Int. J. Mod. Phys. C*, 1998, **9**, 409–419.

[5] C. Chiccoli, S. Guzzetti, P. Pasini, and C. Zannoni, *Mol. Cryst. Liquid Cryst.*, 2001, **360**, 119–129.

[6] R. Memmer and O. Fliegans, *Phys. Chem. Chem. Phys.*, 2003, **5**, 558–566.

[7] L. V. Mirantsev and E. G. Virga, *Phys. Rev. E*, 2007, **76**, 021703.1–7.

[8] D. W. Berreman, *Phil. Trans. Roy. Soc. London. A*, 1983, **309**, 203–216.

[9] F. H. Yu and H. S. Kwok, *J. Opt. Soc. Am. A*, 1999, **16**, 2772–2780.

[10] R. Berardi, L. Muccioli, S. Orlandi, M. Ricci, and C. Zannoni, *J. Phys.: Condens. Matter*, 2008, **20**, 463101.1–16.

[11] M. R. Wilson, *Int. Rev. Phys. Chem.*, 2005, **24**, 421–455.

[12] J. G. Gay and B. J. Berne, *J. Chem. Phys.*, 1981, **74**, 3316–3319.

[13] C. M. Care and D. J. Cleaver, *Reports on Progress in Physics*, 2005, **68**, 2665–2700.

[14] C. Zannoni, *J. Mater. Chem.*, 2001, **11**, 2637–2646.

[15] R. Everaers and M. R. Ejtehadi, *Phys. Rev. E*, 2003, **67**, 041710.1–8.

[16] X. Zheng and P. Palffy-Muhoray, *Phys. Rev. E*, 2007, **75**, 061709.1–6.

[17] R. Berardi, C. Fava, and C. Zannoni, *Chem. Phys. Lett.*, 1995, **236**, 462–468.

[18] R. Berardi, C. Fava, and C. Zannoni, *Chem. Phys. Lett.*, 1998, **297**, 8–14.

[19] R. Berardi, A. P. J. Emerson, and C. Zannoni, *J. Chem. Soc., Faraday Trans.*, 1993, **89**, 4069–4078.

[20] D.-K. Yang and S.-T. Wu, *Fundamentals of Liquid Crystal Devices*, John Wiley and Sons, New York, 2006.

[21] W. L. Jorgensen and J. Tirado–Rives, *J. Phys. Chem.*, 1996, **100**, 14508–14513.

[22] J. P. Ulmschneider, M. B. Ulmschneider, and A. Di Nola, *J. Phys. Chem. B*, 2006, **110**, 16733–16742.

[23] D. Frenkel and B. Smit, *Understanding Molecular Simulations: From Algorithms to Applications, 2nd edition*, Academic Press, 2001.

[24] G. S. Heffelfinger and M. E. Lewitt, *J. Comp. Chem.*, 1996, **17**, 250–265.

[25] G. S. Heffelfinger, *Comp. Phys. Commun.*, 2000, **128**, 219–237.

[26] D. Wolf, P. Keblinski, S. R. Phillpot, and J. Eggebrecht, *J. Chem. Phys.*, 1999, **110**, 8254–8282.

[27] S. J. Plimpton, *J. Comp. Phys.*, 1995, **117**, 1–19.

[28] S. J. Plimpton, 2008, p. URL `http://lammps.sandia.gov/`.

[29] F. Xu, H.-S. Kitzerow, and P. P. Crooker, *Phys. Rev. A*, 1992, **46**, 6535–6540.

[30] W. A. Shurcliff, *Polarized Light: Production and Use*, Harvard University Press, Cambridge, MA, 1962.

[31] B. Witzigmann, P. Regli, and W. Fichtner, *J. Opt. Soc. Am. A*, 1998, **15**, 753–757.

[32] J. A. Barker and R. O. Watts, *Chem. Phys. Lett.*, 1969, **3**, 144–145.

[33] C. Zannoni in *The Molecular Physics of Liquid Crystals;* Academic Press, 1979; pp. 51–83.

[34] T. Mima, T. Narumi, S. Kameoka, and K. Yasuoka, *Mol. Simul.*, 2008, **34**(8), 761–773.

[35] R. Berardi, L. Muccioli, and C. Zannoni, *J. Chem. Phys.*, 2008, **128**, 024905.

[36] D. Micheletti, L. Muccioli, R. Berardi, M. Ricci, and C. Zannoni, *J. Chem. Phys.*, 2005, **123**, 224705.1–10.

[37] R. Berardi, H.-G. Kuball, R. Memmer, and C. Zannoni, *J. Chem. Soc. Faraday Trans.*, 1998, **94**, 1229–1234.

[38] T. Tadokoro, T. Fukazawa, and H. Toriumi, *Japanese J. Appl. Phys.*, 1997, **36**, L1207–L1210.

[39] T. Fukazawa, T. Tadokoro, H. Toriumi, T. Akahane, and M. Kimura, *Thin Solid Films*, 1998, **313–314**, 799–802.

[40] T. Tadokoro, H. Toriumi, S. Okutani, M. Kimura, and T. Akahane, *Japanese J. Appl. Phys.*, 2003, **42**, 4552–4563.

[41] R. Berardi and C. Zannoni, *J. Chem. Phys.*, 2000, **113**, 5971–5979.
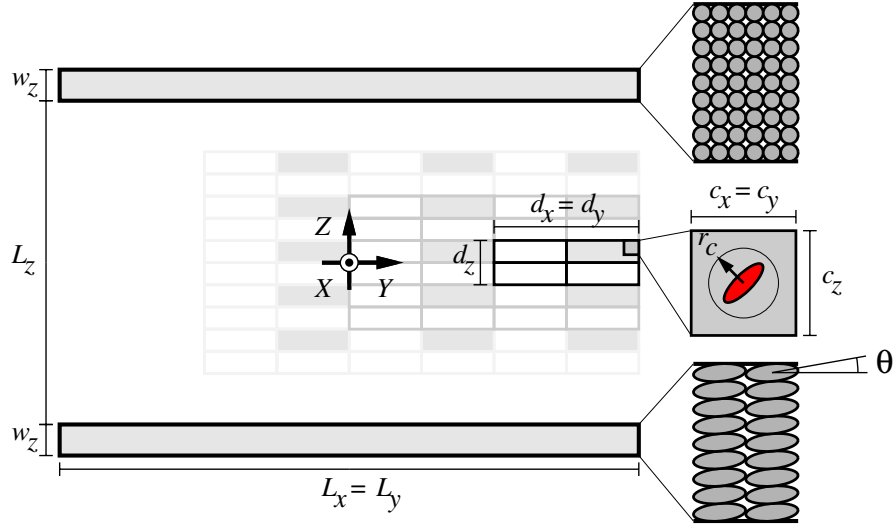
Figure 1: Geometrical scheme showing a vertical section of the TN cell simulated in this work with periodic boundaries in the laboratory X and Y directions. The width, breadth and height of the nematic sample are $L_x = L_y = 167.791\ \sigma_0$, and $L_z = 93.860\ \sigma_0$. The thickness of the confining walls is $w_z = 9\ \sigma_0$, with a pretilt angle $\theta = 5°$. The volume of the entire cell (LC fluid + surfaces) was divided into $4 \times 4 \times 8$ domains with sides $d_x = d_y = 41.948\ \sigma_0$ and $d_z = 13.983\ \sigma_0$. The sizes of the $41 \times 41 \times 27$ linked–cells used to map all the GB particles are $c_x = c_y = 4.092\ \sigma_0$, and $c_z = 4.143\ \sigma_0$. The GB potential cutoff radius $r_c = 4\ \sigma_0$ is also shown.
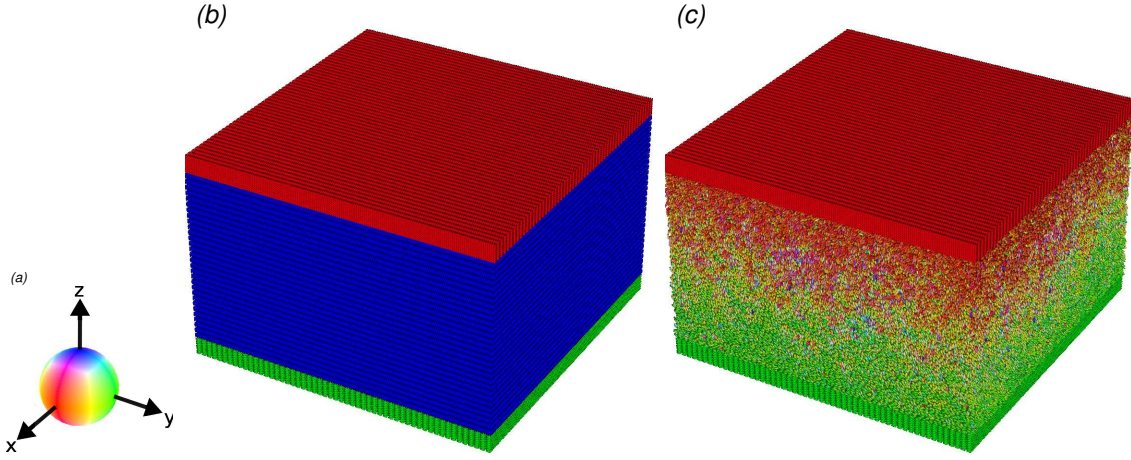
Figure 2: Snapshots of the starting (b) and final (c) MC configurations of the TN cell after a relaxation of 1.76×10^6 sweeps. GB particles are colour coded according to the orientation of molecular $\mathbf{u}_i$ axis with respect to the laboratory frame using the 3D palette of plate a.
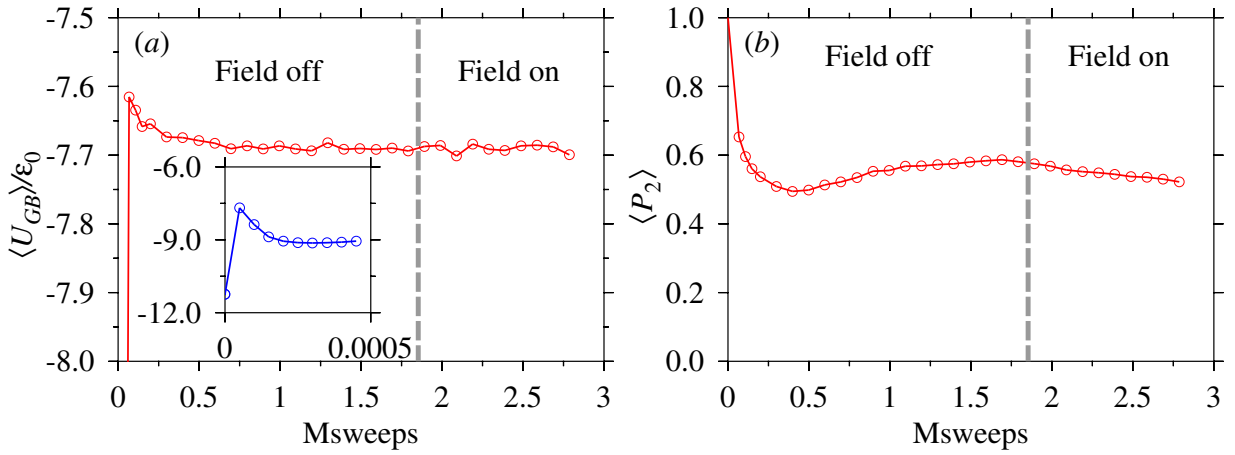
Figure 3: Average GB energy per particle $\langle U_{GB} \rangle / \epsilon_0$ (a), and nematic order parameter $\langle P_2 \rangle$ computed with respect to the overall cell director $\hat{\mathbf{n}}$ (b) as a function of the number of millions of MC sweeps. The vertical dashed line at 1.76×10^6 sweeps marks the end of the relaxation and the beginning of the virtual switching experiment of the central pixel.
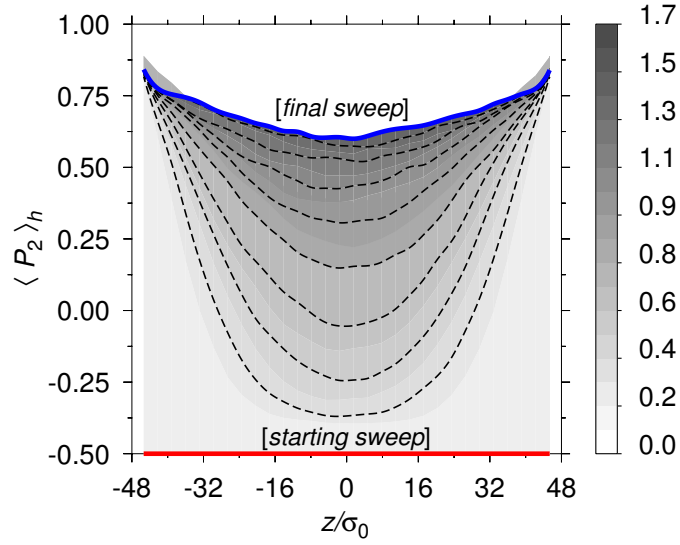
Figure 4: Evolution profiles for the local helical order parameter $\langle P_2 \rangle_h$ (see Equation 2) from the MC relaxation of the uniformly aligned cell. The bottom thick (red) line is for the starting ordered configuration, while the top (blue) one is for twisted organisation after 1.76×10^6 sweeps. Intermediate profiles are shown both as dashed lines every 2×10^5 sweeps and as a greyscale background (see lateral palette). For a perfect helix $\langle P_2 \rangle_h = 1$.
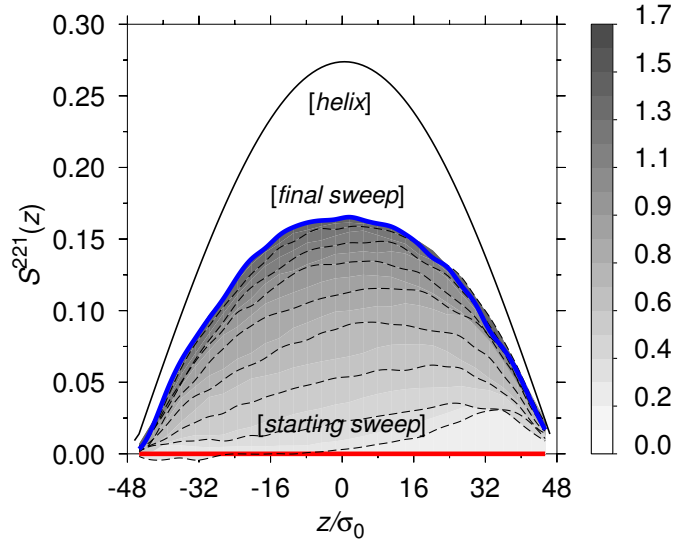
Figure 5: Evolution profiles for the chiral correlation function $S^{221}(z)$ (see Equation 3) from the MC relaxation of the uniformly aligned cell. The thin continuous line is the reference profile for a perfect helix. See the caption of Figure 4 for additional details.
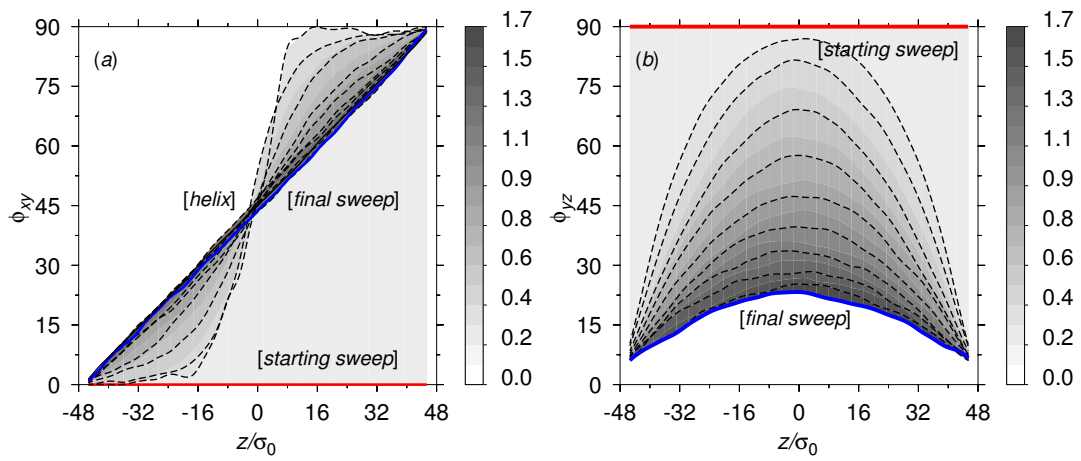
Figure 6: Evolution profiles for the azimuthal angles ϕ_{xy} (a), and ϕ_{yz} (b) defined in the text from the MC relaxation of the uniformly aligned cell. The reference lines for a perfect helix are a straight one bisecting the first quadrant $\phi_{xy} = z$ (a), and a horizontal one $\phi_{yz} = 0$ (b). See the caption of Figure 4 for additional details.
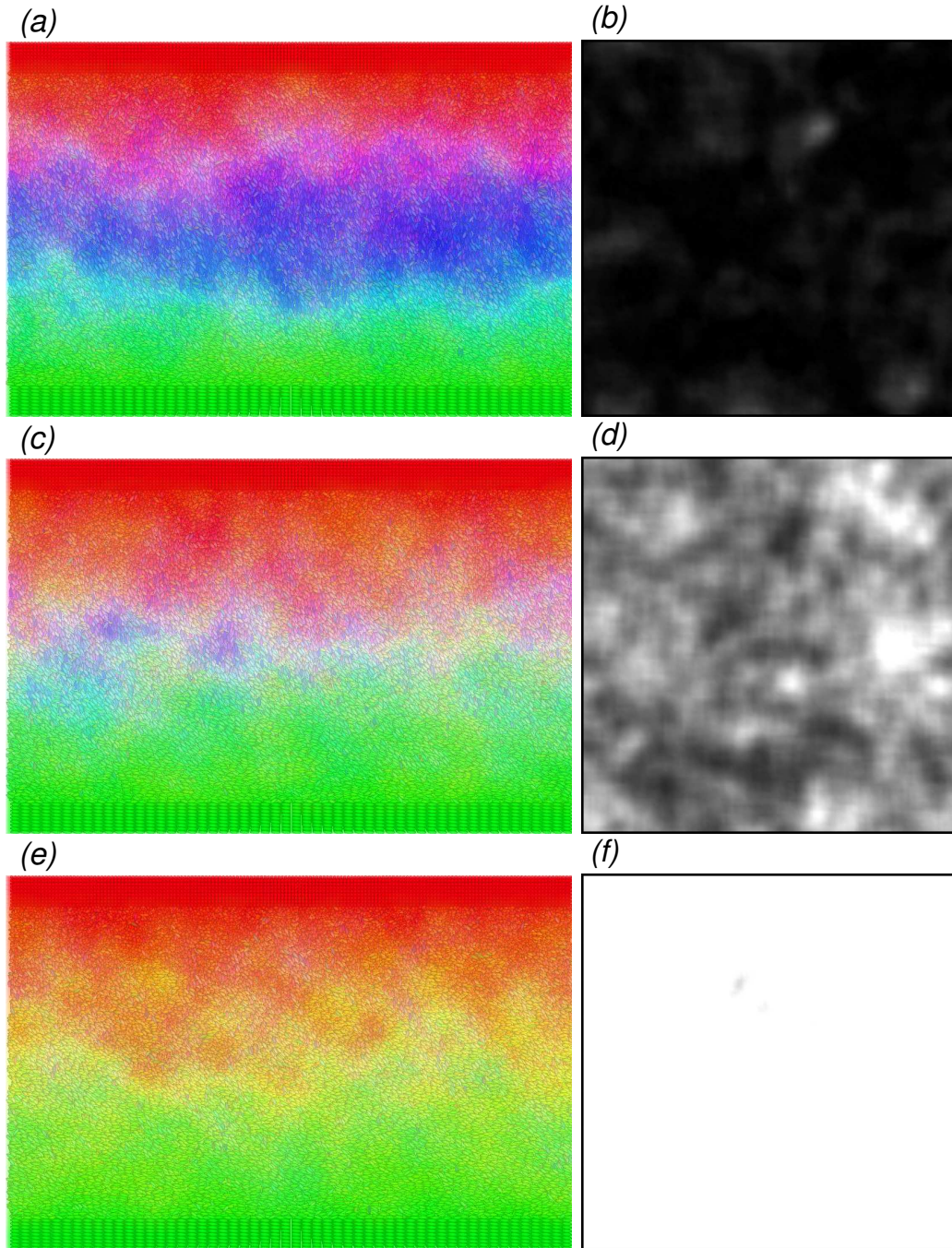
Figure 7: Transverse views of the TN cell from the MC relaxation after 0.46×10^6 sweeps (a), 0.86×10^6 sweeps (c), and 1.63×10^6 sweeps (e) as seen from the laboratory X axis. GB particles are colour coded according to their orientations using the 3D palette of Figure 2, and smoothly rendered to reduce the visual effect of the edges. The corresponding transmittance maps of linearly polarised light across the cell and crossed polarisers (plates b, d, and f), as seen from the laboratory Z axis, are represented by using a linear greyscale palette ranging from 0 (opaque) to 1 (transparent). The overall cell transmittances are 3.5% (b), 30% (d), and 89% (f).
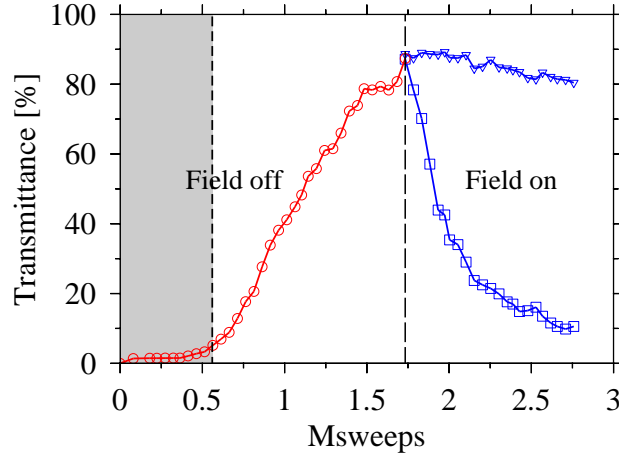
Figure 8: Evolution of the integrated transmittance of linearly polarised light across the simulated TN cell (including crossed polarisers) for the relaxation from uniformly aligned (circles, red), and for the central pixel switching (squares, blue). The transmittance of the external pixels during the field–*on* experiment is also given (triangles, blue). The vertical short–dashed line corresponds to a 5% transmittance, while the long–dashed one at 1.76×10^6 sweeps marks the end of the relaxation and the beginning of the switching experiment.
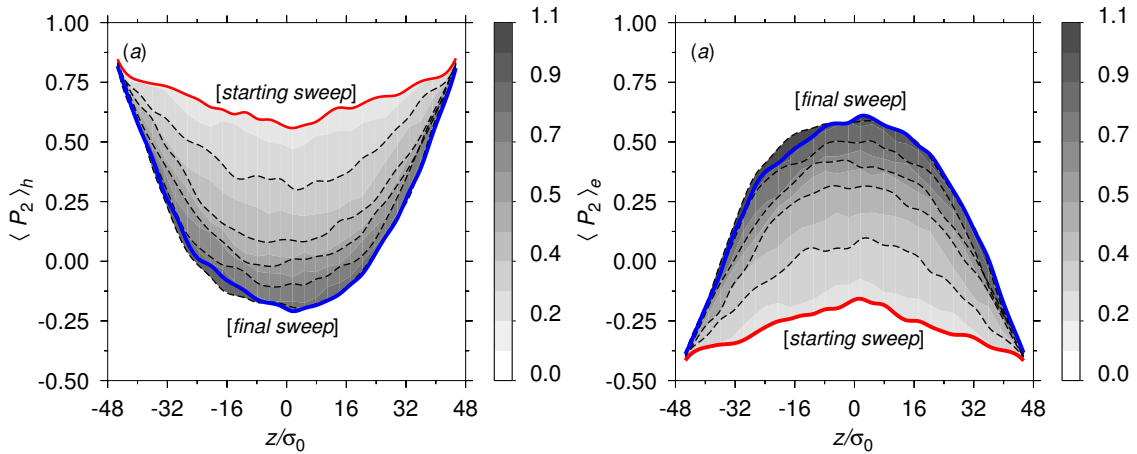

Figure 9: Evolution profiles for the local helical $\langle P_2 \rangle_h$ (a), and for the field direction $\langle P_2 \rangle_e$ (b) order parameters relative to the central field–*on* pixel during the virtual MC switching experiment. The thick lines represent the starting twisted configuration (red), and the final aligned one (blue) after 1.12×10^6 sweeps. Intermediate values are shown both as dashed lines every 2×10^5 sweeps and as a greyscale background (see lateral palettes). For the reference profile of a geometrically perfect helix $\langle P_2 \rangle_h = 1$, and $\langle P_2 \rangle_e = 0$.
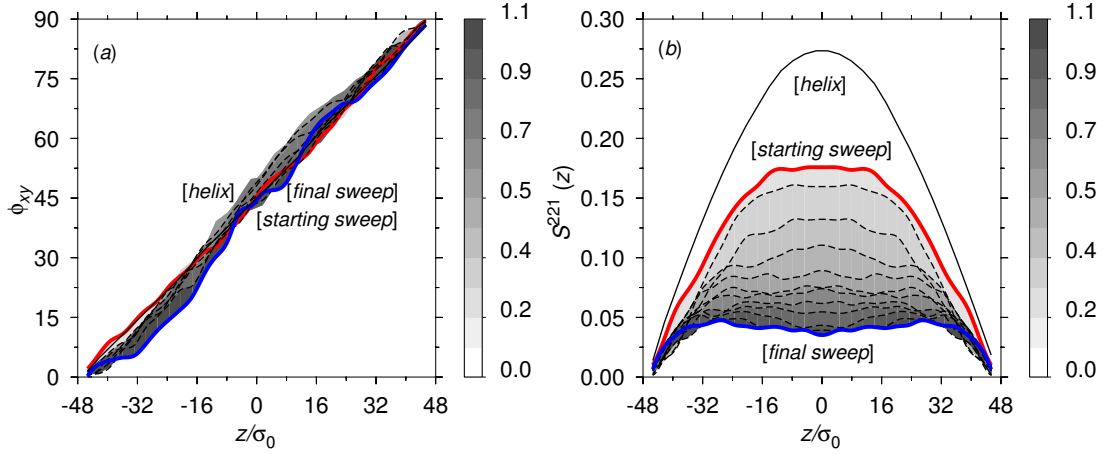
18

Figure 10: Evolution profiles for the azimuthal angles ϕ_{xy} (a), and chiral correlation function $S^{221}(z)$ (b) for the central field–*on* pixel during the virtual MC switching experiment. See Figures 6 and 9 for details.
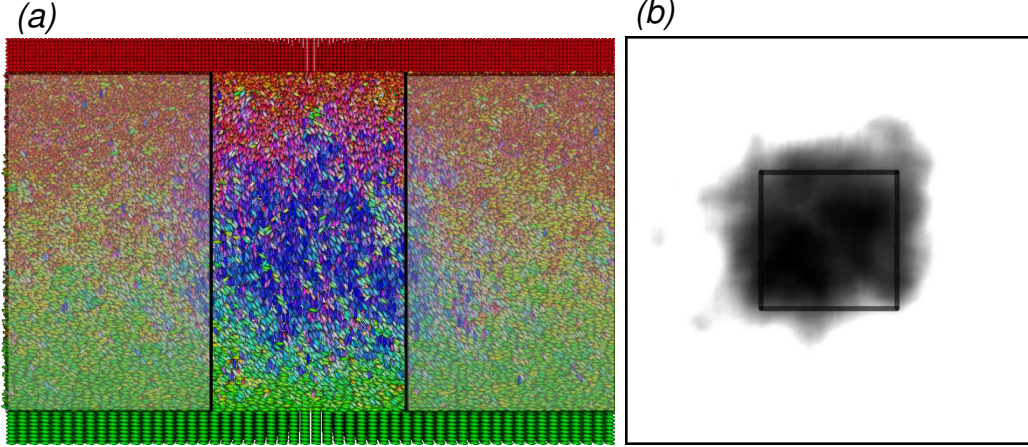

Figure 11: Transverse view of a section of the MC configuration (after 1.12×10^6 sweeps) from the switching *on* experiment of the central pixel (a). To show the organisation of the *on* pixel its particles are rendered without a smoothing filter. Particles are colour coded according to their orientations using the 3D palette of Figure 2. The transmittance map of linearly polarised light is shown in plate b (see Figure 7 for details). Vertical black bars (a) and blue lines (b) delimit the region affected by the external field. The central pixel transmittance is 9%, while the average for the external ones is 79% (b).
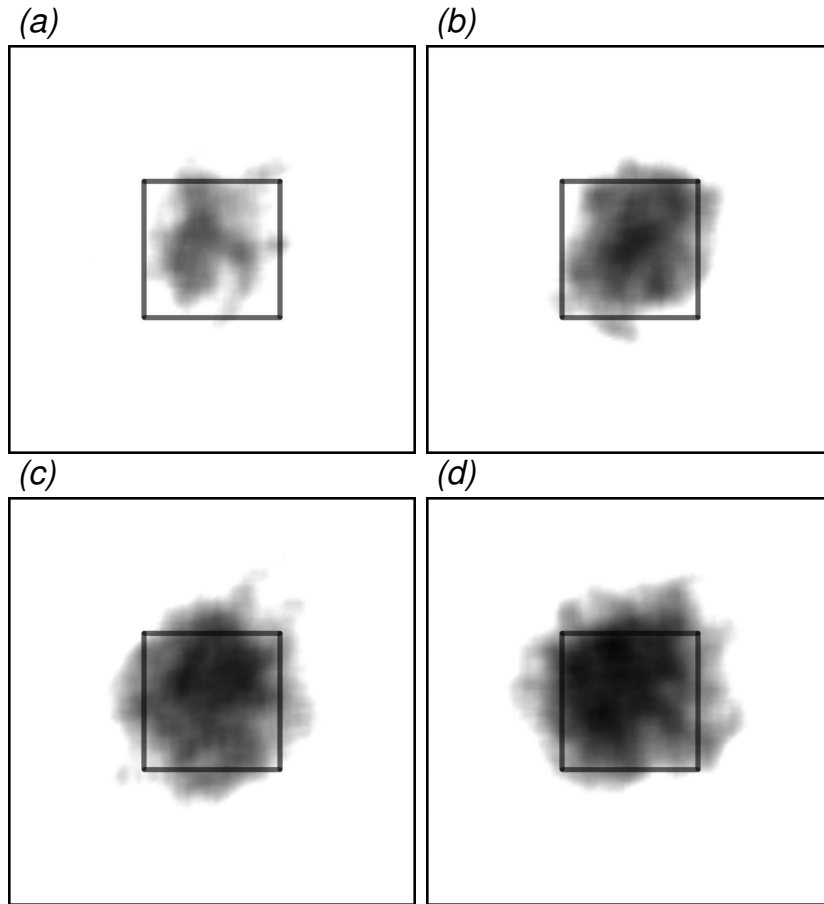
Figure 12: Transmittance maps of linearly polarised light across the cell after 0.2×10^6 sweeps (a), 0.4×10^6 sweeps (b), 0.6×10^6 sweeps (c), and 0.8×10^6 sweeps (d). See Figure 11 for details. The central pixel transmittances are 43% (a), 29% (b), 19% (c), and 15% (d), while the average external ones are 88% (a), 88% (b), 84% (c), and 81% (d).